LIMNOLOGY and OCEANOGRAPHY

ASLO

Limnol. Oceanogr. 67, 2022, 2448–2465

doi: 10.1002/lno.12212

Recycling of dissolved iron in the North Pacific Subtropical Gyre

Nicholas J. Hawco [1,2*] **Shun-Chung Yang** [2,3] **Paulina Pinedo-González** [2,3] **Erin E. Black** [3] **Jennifer Kenyon** [4] **Sara Ferrón** [1] **Xiaopeng Bian** [2] **Seth G. John** [2]

[1]Department of Oceanography, School of Ocean and Earth Science and Technology, University of Hawai'i at Mānoa, Honolulu, Hawaii
[2]Department of Earth Sciences, University of Southern California, Los Angeles, California
[3]Lamont-Doherty Earth Observatory, Palisades, New York
[4]Marine Chemistry and Geochemistry Department, Woods Hole Oceanographic Institution, Woods Hole, Massachusetts

Abstract

The importance of iron as a limiting nutrient in the open ocean is widely recognized, but there is substantial uncertainty about the rate that it cycles in the marine environment. Here, we combine measurements from the water column, sediment traps, and incubations to constrain Fe turnover during summer at Station ALOHA in the North Pacific Subtropical Gyre. Using low levels of ^{57}Fe–^{58}Fe double spike, measured with high precision by multi-collector inductively coupled plasma mass spectrometry, we find Fe uptake rates of 30–60 pM d^{-1} throughout the euphotic zone. Dissolved Fe turnover times are estimated at 10–15 d in the mixed layer and 1–3 d near the deep chlorophyll maximum. Aerosol Fe supply inferred from a thorium isotope mass balance indicates that the dissolved Fe residence time is approximately 6 months in the upper euphotic zone (0–75 m), relative to external sources, and 2 months in the lower euphotic zone (75–150 m). To reconcile these observations, the average Fe atom must be recycled over 25 times at Station ALOHA in both the upper and lower euphotic zones (an "*Fe* ratio" equal to 0.04 and 0.03, respectively), a level of conservation that has only been documented in Fe-limited regions thus far. At steady state, this scenario requires an aerosol Fe solubility of 4.5%, which is similar to dissolution experiments from Pacific Ocean aerosols. Our results suggest that the oligotrophic ocean is capable of recycling iron efficiently even when these ecosystems are not demonstrably iron-limited.

The marine iron cycle is unrivaled in its complexity, both in the diversity of its external sources and in the number of potential reactions it can undergo in seawater (Boyd and Ellwood 2010; Tagliabue et al. 2017). At the same time, such frenetic chemistry still allows for large-scale oceanographic features to emerge, including the propagation of dissolved Fe from coastal and hydrothermal sources and the regeneration of biologically exported Fe in subsurface water masses (Hatta et al. 2015; Resing et al. 2015; Nishioka et al. 2020). Reproducing these features, and identifying their driving mechanisms, has become a priority for biogeochemical modeling of the iron cycle, but many models achieve a similar level of skill by employing very different rates of Fe cycling, which is reflected in modeled Fe residence times varying from less than a decade to over a hundred years (Tagliabue et al. 2016).

Uncertainty over the fluxes controlling the Fe cycle is most pronounced near the ocean surface, which receives the majority of input from atmospheric and coastal sources and is also influenced by biological Fe uptake. By itself, biological uptake might vary by orders of magnitude depending on the extent of Fe bioavailability and the physiological demand associated with photosynthesis, respiration, and nitrogen fixation (Hudson and Morel 1990; Hutchins et al. 1999; Lis et al. 2015). There are only a handful of attempts to balance Fe budgets in the surface ocean, which have mostly emphasized near-daily recycling of dissolved Fe (dFe) in regions like the Southern Ocean and Sub-Antarctic, where phytoplankton are iron-stressed and there is an ecological imperative to recycle Fe in the euphotic zone (Boyd et al. 2005; Ellwood et al. 2020). By contrast, it has been inferred that the iron cycle in regions that are not iron-limited operates more slowly

*Correspondence: hawco@hawaii.edu

Additional Supporting Information may be found in the online version of this article.

Author Contribution Statement: N.J.H., S.-C.Y., P.P.-G., E.E.B., and S.G.J. designed the research. N.J.H., S.-C.Y., P.P.-G., E.E.B., J.K., S.F., and X.B. carried out sample analysis. N.J.H. wrote the manuscript, with contributions from all authors. All authors edited and approved the final version of the manuscript.

due to reduced Fe demand and excess Fe supply (Boyd and Ellwood 2010; Boyd et al. 2017).

Analogous to tracer uptake experiments for nitrate, phosphate, and bicarbonate, several protocols have been developed to determine the rate of Fe uptake in different ocean settings, whereby either stable or radioactive Fe isotopes are added to seawater and their incorporation onto particles after a given time is measured (Hutchins et al. 1999; Maldonado and Price 1999). These techniques have been highly successful in surveying the bioavailability of Fe bound to different organic molecules and the size partitioning of iron uptake, but are often subject to a central drawback: they must be conducted at dFe levels greater than background conditions due to (1) the low specific activity of available radioactive Fe isotopes or (2) the relatively low precision of measuring stable Fe isotope ratios by conventional inductively coupled plasma mass spectrometry (ICPMS). In practice, this often means exogenous Fe addition on the order of 200 to > 1000 pmol L^{-1}, which likely does not fully equilibrate with the strong ligand pool, saturates high affinity Fe transport pathways, and increases rates of Fe precipitation and scavenging onto particulate matter. Although exceptions exist (e.g., Hassler et al. 2011), the iron uptake rates derived from these measurements cannot be easily related to background conditions.

Here, we present results from stable Fe isotope uptake experiments that leverage the high precision of multi-collector ICPMS (MC-ICPMS). Measurement of Fe isotope ratios by MC-ICPMS enables smaller amounts of stable Fe isotopes to be used in uptake experiments, on the order of 10 pM, which is only a fraction of the dissolved Fe concentration. We apply this method to examine the profile of dissolved Fe uptake and turnover time throughout the euphotic zone at Station ALOHA, the site of the Hawaii Ocean Time-series (HOT) within the North Pacific Subtropical Gyre. In combination with external Fe fluxes derived from sediment traps and thorium isotopes, we calculate both the "turnover time" of dFe, describing the tempo that dFe exchanges with Fe in labile particulate matter by biological uptake and adsorption. This is compared to the dFe "residence time," which characterizes the timescale that dFe is exported from the upper and lower segments of the euphotic zone and replaced by new iron from aerosol deposition. Together, these measurements demonstrate a high efficiency of iron recycling in this oligotrophic ecosystem.

Methods

Oceanographic samples were collected onboard the R/V *Kilo Moana* at Station ALOHA (22.45°N, 158.0°W) during June 2019. Trace metal clean sampling was conducted using a powder coated Al framed rosette (Seabird), with 8-L external spring bottles (Ocean Test Equipment). Contextual measurements of fluorometric chlorophyll *a* and flow cytometry enumeration of phytoplankton types followed standard HOT methods (https://hahana.soest.hawaii.edu/hot/protocols/). Measurements of gross oxygen production (GOP) by the $H_2{}^{18}O$ incubation technique were performed as described previously (Ferrón et al. 2016). On 18 June and 21 June, seawater samples were collected before dawn in triplicate at different depths (5, 25, 45, 75, 100, and 125 m), spiked with $H_2{}^{18}O$ (97.6% ^{18}O, Medical Isotopes), and incubated in situ until dusk using a free-drifting array (~ 14 h). The isotopic enrichment of dissolved O_2 was subsequently measured on board (within 24 h of recovery) by membrane inlet mass spectrometry (Ferrón et al. 2016).

Total dissolvable iron (tdFe) concentrations were measured in unfiltered 1 L samples by Nobias PA-1 extraction and measurement by Element 2 ICPMS (Thermo Scientific) as described in Hawco et al. (2020*b*). A 20 pM reagent blank was subtracted. There are no seawater standards for tdFe measurements but we have reproduced dFe concentrations in GEOTRACES seawater standards using identical isotope dilution methods in recent studies (Pinedo-González et al. 2020; Hawco et al. 2021*a*). Our results are also comparable to past measurements at Station ALOHA (*see* "Discussion" section; Boyle et al. 2005; Fitzsimmons et al. 2015*b*).

Protocols for applying a combined ^{57}Fe and ^{58}Fe double spike (Fe_{DS}) and MC-ICPMS analyses for Fe uptake experiments are described below. A schematic of the procedures for conducting incubations at sea, as well as sample processing in the lab is presented in Supporting Information Fig. S1.

Preparation of isotope spike

^{57}Fe and ^{58}Fe used in the Fe_{DS} isotope spike were originally acquired as a solid oxide phase from Isoflex USA, combined, purified, and quantified as described in Conway et al. (2013). To prevent inadvertent nitrate addition from nitric acid, the Fe_{DS} solution was evaporated and resuspended in 0.01 M hydrochloric acid (HCl) to a concentration of 300 nM Fe, and stored at room temperature in the dark until use at sea (< 1 month). Measurement of the Fe_{DS} solution before the cruise and several months afterward indicated minimal loss of Fe (0–20%) during storage under mildly acidic conditions.

Incubation methods and sample processing

All plasticware used in the incubations were subject to standard cleaning procedures. Bottles were soaked for 24 h in 1% citranox detergent, rinsed thoroughly with 18.2 MΩ water, followed by a 1 week soak in 10% HCl and several rinses in 18.2 MΩ water. All materials were double bagged and opened only in particle-free spaces within a laboratory van bubble. A "pre-incubation" was conducted to equilibrate added inorganic Fe (i.e., Fe′) with iron binding ligands in seawater. Water collected at several depths from a profiling cast ~ 21 h prior to the start of the incubation was filtered through a 0.2-μm polyethersulfone (Supor) capsule filter into 60-mL polycarbonate (PC) bottles (Nalgene), conditioned with triplicate seawater rinses prior to filling. Double spike solution (100 μL) was

added and allowed to equilibrate in the dark at room temperature for > 12 h. Based on a 300 nM spike diluted to 0.13% of the preincubation volume, the added Fe_{DS} concentration was estimated to be 415 pM.

The Fe uptake experiment was conducted in 2-liter PC bottles mounted at six depths on a surface tethered in situ array (18 June). Array set up and deployment procedures were analogous to those used for primary production arrays by the HOT program (Karl et al. 2021). Prior to deployment, a second rosette cast was performed at 0200 h (local time) to collect water for the incubation. As for the GOP experiments, presunrise sampling is important for capturing the entire photosynthetic period and minimizing perturbations to cells associated with confinement in bottles. To avoid light-shock to phytoplankton photosystems, all incubation set-up took place in near-darkness under red light. After rinsing the 2-liter bottles with seawater, the entire Fe_{DS}-spiked preincubation was added and the remaining volume was filled completely with unfiltered seawater. Bottles were affixed to a custom-built rack and the array was deployed before sunrise. A second incubation was performed on 21 June with water collected from 15 m depth in an on-deck flow-through incubator shaded to light levels matching the mixed layer. Following recovery after sunset, bottles were harvested by vacuum filtration. Particles were filtered onto a 0.2-μm 47-mm Supor filter and filtrate was collected in a 1-liter low density polyethylene bottle. After returning to the lab, the filtrate was acidified to pH 1.8 by addition of distilled HCl and allowed to rest for > 2 months.

Filtered seawater and particles were processed analogously to standard Fe isotope protocols. Filters were digested in 50% HNO_3 for > 12 h in perfluoroalkoxy (PFA) vials (Savillex) at 95°C. This procedure was chosen to minimize processing blanks and should not solubilize aluminosilicate bound Fe (Planquette and Sherrell 2012), which is not expected to exchange with dissolved Fe on daily timescales. After removal of filters, the digest was subsequently evaporated to dryness. Filtered, acidified seawater from the incubations was extracted with Nobias PA-1 resin using the batch extraction technique described by Conway et al. (2013). Both dissolved and particulate samples were re-digested in a 1 : 1 solution of concentrated HCl and HNO_3 (100 μL each), heated to 95°C for 2 h, evaporated to dryness, and resuspended in 250 μL 10 M HCl in preparation for column chemistry. Fe was purified using micro-columns with AG-MP1 resin (Bio-RAD), as in Conway et al. (2013), dried, and resuspended in 0.1 M HNO_3 for analysis by MC-ICPMS.

Measurement by MC-ICPMS

The isotopic composition of Fe was measured on a Neptune Plus MC-ICPMS (Thermo Scientific) at the College of Marine Science at the University of South Florida. Samples were introduced through an Apex-IR introduction system with a 100–150 μL min^{-1} PFA nebulizer. A Jet sampler cone and an "x-type" skimmer cone were used to maximize sensitivity. Instrument settings and data acquisition followed Hawco et al. (2020*b*). Beams for ^{53}Cr, ^{54}Fe, ^{56}Fe, ^{57}Fe, ^{58}Fe, and ^{60}Ni were measured simultaneously with data collected in 30 4.2-s cycles.

Isotope ratios were derived by sample standard bracketing whereby the primary IRMM-14 standard solution was analyzed every four samples, along with a 0.1 M HNO_3 blank. The concentration of natural abundance Fe (Fe_{NA}) in a sample was calculated as:

$$[Fe_{NA}] = f_{56} \times \frac{V_{56Fe}}{S_{56Fe}}, \quad (1)$$

where f is the fraction of Fe as ^{56}Fe in the IRMM-14 standard, V_{56Fe} is the signal intensity of ^{56}Fe for a given samples (in volts) and S_{56Fe} is the sensitivity of ^{56}Fe in volts (ppb Fe)$^{-1}$ for IRMM-14. Correction for isobaric interferences from ^{54}Cr and ^{58}Ni was performed assuming natural abundance Cr and Ni isotope ratios, assuming the same instrumental mass bias for Cr, Ni, and Fe. Analysis blanks were subtracted from all Fe isotope beams. Variation in the analyses of the IRMM-14 standard was 0.41‰ for the ^{54}Fe/^{56}Fe ratio, 1.06‰ for ^{57}Fe/^{56}Fe and 5.89‰ for ^{58}Fe/^{56}Fe (1 SE; $n = 24$). Although this level of uncertainty would not allow for examination of natural Fe isotopic variation, it is sufficient for the tracer studies described here.

The concentration of spike (Fe_{DS}) was calculated according to the equation:

$$[Fe_{DS}] = [Fe_{NA}] \times \Big(\left(R_{57:56,sample} - R_{57:56,IRMM-14}\right) + \left(R_{58:56,sample} - R_{58:56,IRMM-14}\right) \Big), \quad (2)$$

where $R_{57:56}$ is the ratio of ^{57}Fe/^{56}Fe in the sample and the IRMM-14 standard. Lastly, we note that the use of a double spike is not strictly necessary, but this was chosen to limit cross-contamination when analyzing natural Fe isotope variations that employ the same Fe_{DS} to correct for instrument mass bias. Because our Fe_{DS} contains near equal amounts of ^{57}Fe and ^{58}Fe, proportional contribution from each isotope served as a check on the validity of [Fe_{DS}] calculated by Eq. 2.

Th isotope tracers

Samples from nine depths in the upper 300 m were collected on 22 June for quantification of ^{230}Th and ^{232}Th. Seawater was filtered through a 0.2-μm Supor filter and collected in 4-liter cubitainers. After the cruise, samples were extracted, purified, and analyzed by ICPMS at the Lamont Doherty Earth Observatory according to standard procedures, recently updated and described in detail by Pinedo-González et al. (2021). In general, measurements agree with prior work at Station ALOHA (Hayes et al. 2015), as described in "Results" section.

Sediment trap and McLane pump deployment

Sinking particles were collected over a 3-d period using a surface tethered array at 75, 150, and 300 m. Two array deployments were conducted. Cylindrical particle interceptor traps (PITs) were filled with a trace-metal-clean brine and fastened to a vinyl "cross" routinely used by the HOT program and attached to a metal-free spectra line. To make the 10% brine, 0.2 μm filtered trace-metal-clean seawater was supplemented with high-purity sodium chloride (99.999% trace metals basis, Sigma-Aldrich). Roughly 2 liters of brine were poured into acid-washed PITs, which were capped by an additional 500 mL of trace metal clean seawater.

Recovered PITs were capped, homogenized, and split. Half of the sample was filtered through a 0.2-μm Supor filter under vacuum filtration for trace metal analysis. Prior to filtration, a 0.5 × 0.5-mm nylon mesh was used to screen out large zooplankton. Filters were digested according to the HF/HNO_3 total digestion method of Planquette and Sherrell (2012) and analyzed by ICPMS at USC. The second half of the sample was filtered onto a QM-A filter for particulate carbon measurements as described in Black et al. (2018).

Two large volume pump (McLane) deployments were also conducted at 25 and 100 m for the collection of suspended particles. Trace-metal-clean pump heads were deployed with 0.8-μm Supor membranes and 51-μm Nytex filters and pumps were attached to metal free line. Only the small size fraction (< 51 μm) is reported here because of uncertainties associated with filter blanks for the Nytex filters. It is well established that Station ALOHA is dominated by small particles (White et al. 2015), so exclusion of this fraction is unlikely to strongly influence reported values. After recovery, filters were split and digested using the same total digestion as for the sediment trap samples.

Results

Incubation design

Incubations were conducted at Station ALOHA and designed so that ~ 425 pM of Fe_{DS} added to "preincubations" would not exceed the concentration of excess Fe-binding ligands in seawater. Recent measurements at Station ALOHA indicate that excess ligand (L) concentrations vary between 400 and 1200 pM and are similar throughout the euphotic zone (Fitzsimmons et al. 2015*b*; Bundy et al. 2018). Fe speciation was not measured on the June 2019 expedition but the timescale of the pre-incubation (~ 12 h) was chosen to be similar to competing ligand exchange experiments used in these and other voltammetry studies. For instance, the 2nd-order rate constants for unchelated Fe (Fe′) and L binding observed in other regions (k_f ~ 10^6 M^{-1} s^{-1}; Witter et al. 2000; Witter and Luther III 1998) imply that most of the added Fe was likely chelated by strong ligands within 2 h, even if a fraction of the Fe ligand pool may take longer to reach equilibrium (Laglera and Filella 2015).

Assuming no loss of Fe to bottle walls during pre-incubation, Fe_{DS} in the main incubation would be 15 pM, roughly 3% of the 445 pM dFe measured in the mixed layer (15 m depth). When the concentration of Fe_{DS} was calculated using Eq. 2, the isotope ratios measured from the on-deck incubation indicated dissolved Fe_{DS} was 7.0 ± 1.7 pM, and particulate Fe_{DS} was 0.55 ± 0.12 pM (Table 1). The sum of these pools, 7.5 pM, was only 50% of the Fe_{DS} added to pre-incubation bottles. A similar percentage was estimated for all experiments (Supporting Information Table S1). At pH = 8.1, the solubility of Fe′ with respect to amorphous Fe oxyhydroxides is on the order of 10 pM (Liu and Millero 2002; Rose and Waite 2003), and it is suspected that precipitation

Table 1. Example measurements from the on-deck incubation (~ 15 m conditions). Values in per mille notation are shown in parentheses. Data correspond to a dFe uptake rate of 24.6 ± 3.6 pM d^{-1} and a turnover time of 18.0 ± 2.8 d. See Table 2 for other incubations.

	^{56}Fe, volts	54/56	57/56	58/56	Fe_{NA} (pM)	Fe_{DS} (pM)
IRMM-14 ± 1SD		**0.0600 ± 0.0001**	**0.0237 ± 0.0001**	**0.0032 ± 0.0001**		
(‰)		(± 2.0‰)	(± 5.2‰)	(± 28.8‰)		
Blank (*n* = 3)	*0.024 ± 0.02*				*9.2 ± 0.8*	*0.05 ± 0.07*
dFe A	1.43	0.0600	0.0281	0.0073	482	4.1
dFe B	1.33	0.0599	0.0296	0.0088	449	5.2
dFe C	1.28	0.0600	0.0300	0.0091	431	5.2
Average ± 1SD	**1.35 ± 0.08**	**0.0600 ± 0.0000**	**0.0292 ± 0.0010**	**0.0084 ± 0.0010**	**454 ± 26**	**5.2 ± 0.6**
(‰)		(− 1.2 ± 0.3‰)	(232 ± 42‰)	(1627 ± 299‰)		
Blank (*n* = 6)	*0.74 ± 0.17*				*62 ± 14*	*0.13 ± 0.03*
pFe A	3.64	0.0599	0.0243	0.0038	305	0.38
pFe B	3.03	0.0599	0.0245	0.0040	254	0.38
pFe C	3.31	0.0600	0.0256	0.0040	278	0.47
Average ± 1SD	**3.33 ± 0.31**	**0.0600 ± 0.0000**	**0.0245 ± 0.0001**	**0.0039 ± 0.0001**	**279 ± 26**	**0.41 ± 0.05**
(‰)		(− 1.3 ± 0.3‰)	(31.3 ± 4.9‰)	(230 ± 33‰)		

There have been no additional statistical tests performed on data in this table, aside from calculation of mean and standard deviation.

and adsorption of particulate Fe_{DS} to bottle walls occurred during preincubation when added Fe_{DS} was initially 10-fold greater than the solubility limit and not equilibrated with ligand pools. At high initial Fe′, the kinetics for Fe′ precipitation ($k_f > 10^7$ M^{-1} s^{-1}; Pham et al. 2006; Rose and Waite 2003) are probably faster than Fe′ binding to organic ligands (~ 10^6 M^{-1} s^{-1}; Witter and Luther III 1998). This highlights the important role for the preincubation step for ensuring stable Fe speciation at the start of the uptake experiment.

Detection of added ^{57}Fe and ^{58}Fe by MC-ICPMS

Fe uptake incubations were initiated upon dilution of "preincubated" Fe_{DS} to unfiltered seawater. Measurement by MC-ICPMS was capable of resolving isotopic variation at low levels of spike addition (Table 1). For the on-deck incubation (waters sampled at 15 m), the ^{57}Fe : ^{56}Fe ratio of dFe was 0.0292 ± 0.0010 (1 SD, n = 3), which is significantly enriched relative to the natural abundance ^{57}Fe : ^{56}Fe of the IRMM-14 isotope standard (0.0237 ± 0.0001; 1 SD, n = 24). The corresponding particulate ^{57}Fe : ^{56}Fe was 0.0245 ± 0.0001 (1 SD, n = 3), also in excess of the natural abundance ratio. The deviation from natural abundance is equivalent to a $\delta^{57}Fe_{IRMM}$ of 232 ± 42‰ and 33.1 ± 4.9‰ for the dissolved and particulate samples, respectively. Meanwhile, the standard deviation of IRMM-14 during this analysis session was 5.2‰ for $\delta^{57}Fe_{IRMM}$ (n = 24), which can be used to estimate a detection limit for this analysis: 15.6‰ (i.e., 3 SD). Excluding three replicates identified as contaminated (*see* Supporting Information Table S1), all samples exceeded this detection limit. Ratios of ^{58}Fe : ^{56}Fe, the former also added as part of the Fe_{DS}, were similarly robust (Table 1). Importantly, mean values of $\delta^{56}Fe_{IRMM}$ (relative to ^{54}Fe) in both dissolved (+ 1.2‰) and particulate (+ 1.3‰) samples did not exceed the standard deviation of IRMM at natural abundance (± 2.0‰, n = 24), indicating that isotope fractionation during measurement did not meaningfully bias measurements of added ^{57}Fe and ^{58}Fe. Natural variation in the seawater Fe isotopic composition in dissolved and particulate samples is small (−1‰ < δ^{56}Fe < +1‰; Conway and John 2014, 2015) compared to magnitudes generated through Fe_{DS} addition and should not influence measured values in uptake experiments.

Determining Fe uptake rates in the mixed layer from double spike incubations

The timescale (τ) for turnover of added Fe_{DS} can be calculated as:

$$\tau_{dFe_{DS}} = \left(\frac{pFe_{DS} + dFe_{DS}}{pFe_{DS}}\right) \cdot \Delta t, \quad (3)$$

where Δt is the time interval of the incubation, in days (a Δt of 1 d is used here based on time from Fe_{DS} addition to completion of sample filtration). If it is assumed that added Fe_{DS} has equilibrated with the entire 445 pM pool of dFe, the bulk Fe uptake rate can be calculated as:

$$\rho_{dFe} = \frac{[dFe_{NA}]}{\tau_{dFe_{DS}}}, \quad (4)$$

where ρ_{dFe} has units of mol L^{-1} d^{-1}. Calculated as such, the dFe uptake rate from the on-deck incubation with water from the mixed layer (15 m) was 24.6 ± 3.6 pM d^{-1} and the corresponding dFe turnover time was 18 ± 3 d. A very similar result was also obtained from in situ incubations deployed in the mixed layer (dFe = 445 pM, ρ_{dFe} = 31 ± 12 pM d^{-1}, τ_{FeDS} = 16 ± 6 d), indicating that these rates were relatively steady over short timescales (Table 2).

Fe uptake in the lower euphotic zone

A local minimum in dFe is frequently observed in the lower euphotic zone of subtropical gyres, especially near the deep chlorophyll maximum (DCM) (Fitzsimmons et al. 2015*b*; Hawco et al. 2021*a*). During June 2019, dFe at 100 m was 71 ± 10 pM (Fig. 1), similar to an average value of 65 ± 22 pM over 90–130 m at ALOHA from Fitzsimmons et al. (2015*b*). Fe uptake incubations conducted under in situ light and temperature regimes by a surface tethered array led to recovery of 7.2 ± 0.7 pM spike from dissolved and particulate phases,

Table 2. Profile of Fe uptake rates at Station ALOHA. Values indicate mean ± SD.

Depth	dFe, pM	ρ_{dFe}, pM d^{-1}	τ_{FeDS}, days	Fe : C uptake ratio, μmol : mol
On deck (21 June 2019)				
15 m (n = 3)	445 ± 26	24.6 ± 3.6	18.0 ± 2.8	46.2 ± 9.1
In situ (18 June 2019)				
5* m (n = 3)	445 ± 16	31.3 ± 12	14.2 ± 5.4	47.9 ± 20.3
25 m (n = 2)	419 ± 47	47.6 ± 13	8.8 ± 2.5	58.2 ± 16.9
45 m (n = 2)	200 ± 24	51.9 ± 4.9	3.9 ± 0.6	80.9 ± 9.2
75 m (n = 2)	83 ± 11	51.0 ± 4.7	1.6 ± 0.3	116 ± 11.6
100 m (n = 3)	71 ± 10	46.5 ± 9.9	1.5 ± 0.4	188 ± 42.4
125 m (n = 3)	137 ± 34	58.2 ± 13.1	2.4 ± 0.8	618 ± 144

*Waters collected at 15 m, incubated at 5 m. Both depths fall within the surface mixed layer.

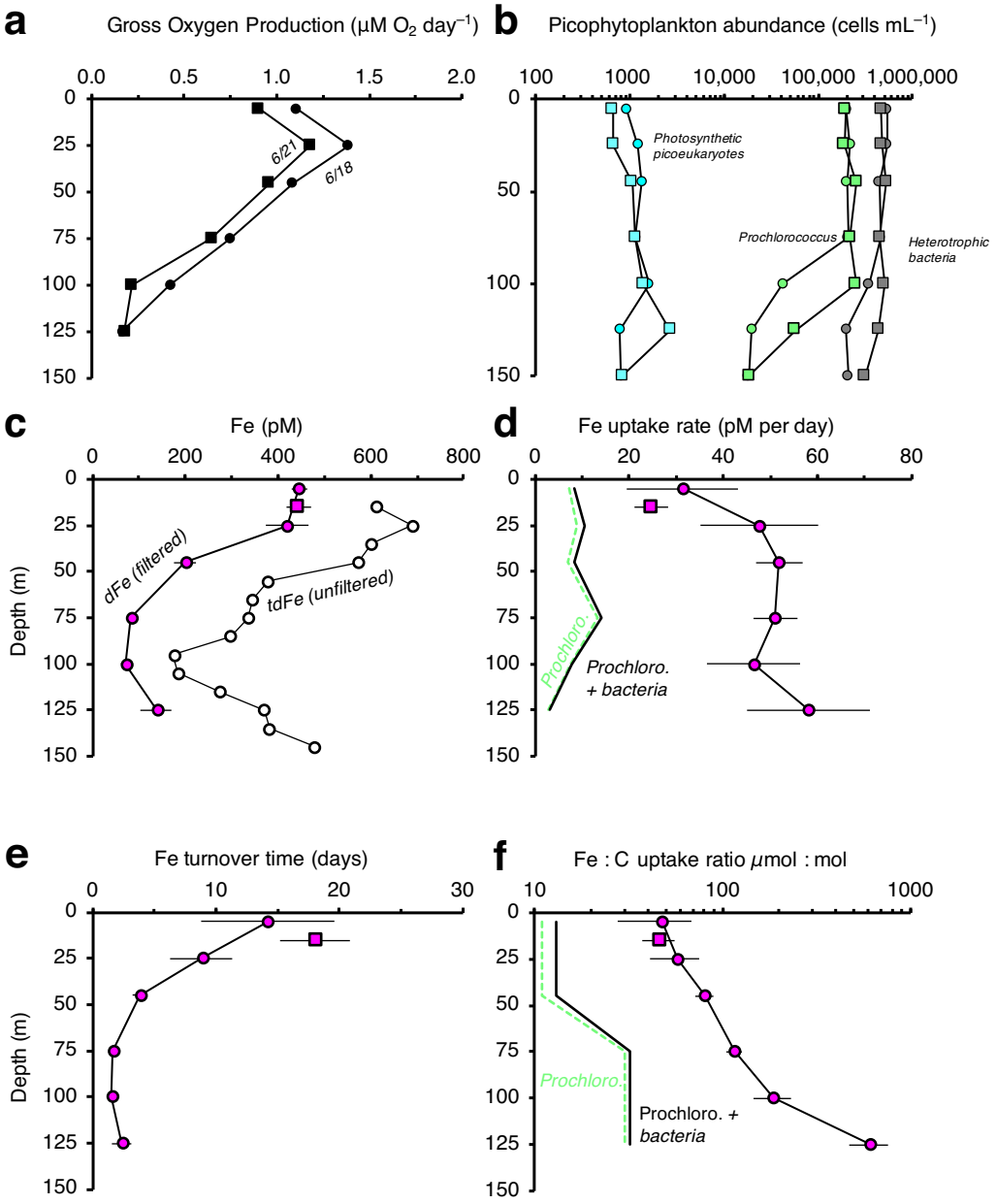

Fig. 1. Productivity and dissolved iron uptake at Station ALOHA in June 2019. (**a**) GOP and (**b**) picoplankton abundance obtained on 18 June (circles) and 21 June (squares). (**c**) Dissolved iron concentrations measured after Fe uptake incubations for the in situ experiments on 18 June 2019 (pink) and the on deck experiment on 21 June (cyan). Note that the tdFe profile (open circles) was collected on a separate cast. (**c**) Iron uptake rates. Expected uptake rates needed to support *Prochlorococcus*-dominated primary production (green dashed line) is estimated from rates of GOP, an empirical O_2 : C ratio of 1.7 at Station ALOHA (Ferrón et al. 2016), and limiting Fe : C ratios of high- and low-light adapted *Prochlorococcus* (Hawco et al. 2020*a*, 2021*b*). Fe demand by heterotrophic bacteria (dotted black line) is estimated under the assumption of ecosystem metabolic balance, a bacterial growth efficiency of 0.26 and a representative Fe : C ratio (Tortell et al. 1996). Calculations are described further in the "Discussion" section. (**d**) Dissolved Fe turnover times. (**e**) Fe : C uptake ratios from incubations. The shift in Fe : C of *Prochlorococcus* represents the expected dominance of low-light adapted ecotypes near the DCM.

meaning that Fe_{DS} increased background dFe by 10%. In contrast to mixed layer incubations, more Fe_{DS} was measured in the particulate phase at 100 m (4.9 ± 0.6 pM) than in the 0.2 μm filtrate (2.4 ± 0.3 pM), implying a turnover time of 1.5 ± 0.4 d from Eq. 3. Equivalent turnover times were also observed at 75 and 125 m (1.6 ± 0.3 and 2.2 ± 0.7 d, respectively; Table 2). Despite the order of magnitude difference in turnover time between the mixed layer and the DCM (Fig. 1), the corresponding bulk Fe uptake rate at 100 m, 48 ± 10 pM d^{-1}, was similar to the surface. Indeed, no significant difference in bulk Fe uptake rate was observed throughout the upper 125 m ($p > 0.05$, one-way ANOVA).

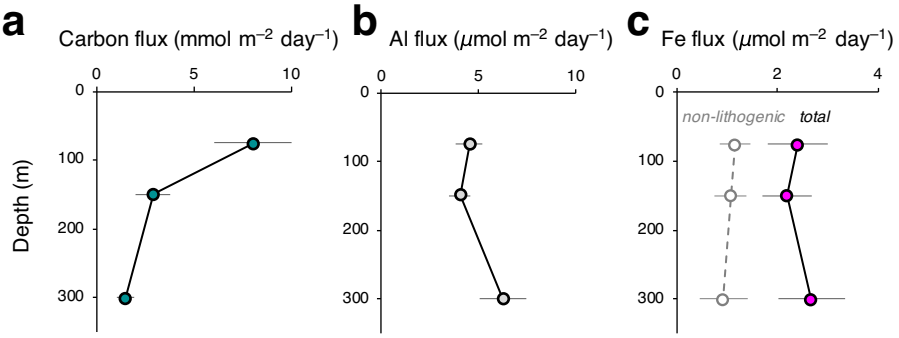

Fig. 2. Sediment trap fluxes of carbon (**a**), aluminum (**b**), and iron (**c**) during June 2019. Circles represent averages of two 3-d deployments, each with three PIT traps. Error bars reflect 1 SD. The non-lithogenic Fe flux is calculated as total Fe flux — 0.28 × Al flux, where 0.28 reflects the Fe : Al ratio for Asian dust (*see* the main text).

Sediment trap Fe fluxes and suspended particulate Fe

Steady patterns of Fe export throughout the water column were observed during two sediment trap deployments within and below the euphotic zone (Fig. 2). For all depths, measured Fe : Al ratios averaged 0.50 ± 0.09 mol mol^{-1} (Table 3), but decreased slightly in the 300 m traps (0.43 mol mol^{-1}) compared to the 75 and 150 m traps (0.53 and 0.55, respectively). A similar pattern was observed previously at Station ALOHA during the VERTIGO program in June and July 2004, where sinking particles had an Fe : Al ratio of 0.46 at 150 m and 0.36 at 300 m (Lamborg et al. 2008). Assuming lithogenic aerosols contain 8% Al by mass, scaling of the June 2019 Al flux at 150 m indicates recent rates of dust deposition on the order of 1.3–1.4 mg m^{-2} d^{-1}, which is broadly in line with mean dust deposition rates predicted by atmospheric models for this region (~ 0.3 g m^{-2} yr^{-1} or 0.8 mg m^{-2} d^{-1} from the DustCOMM model; Kok et al. 2021). The increase in Al flux at 300 m may indicate ~ 50% more deposition in the weeks prior to the cruise, which would be consistent with a March–May peak in atmospheric dustiness for the central Pacific (Prospero et al. 2003).

The Fe : Al ratios in the shallow traps are also similar to the mean Fe : Al ratio of 0.53 for North Pacific aerosols reported by Buck et al. (2006), which is notable because it exceeds the observed composition expected from Asian dust storms and continental crust generally (0.28 mol mol^{-1}; Arimoto et al. 2004). The Buck et al. (2006) dataset itself trends toward 0.28 mol mol^{-1} when sampling Asian dust events over the North Pacific, and so the higher mean value may indicate a significant source of anthropogenic or biomass-derived Fe to the open ocean that is more apparent in low-dust periods. Regardless, subtraction of the lithogenic component using the 0.28 Fe : Al endmember ratio indicates that sinking fluxes of non-lithogenic Fe decreased by ~ 20% from 75 to 300 m, which stands in contrast to the ~ 80% attenuation of C flux over the same depth range (Fig. 2). A flux of non-lithogenic Fe at 150 m of 1.07 ± 0.32 μmol m^{-2} d^{-1} (1 SD, n = 6) is also similar to a flux of 1.47 μmol m^{-2} d^{-1} observed by Lamborg et al. (2008) when the same endmember Fe : Al correction is applied (Table 3). Collection of suspended particulate samples at 25 and 100 m depth also indicated elevated Fe, relative to Al (Fe : Al > 1; Supporting Information Table S2).

Thorium based fluxes of dissolved Fe

The profile of dissolved ^{230}Th and ^{232}Th was also measured at Station ALOHA during the 2019 sampling period (Fig. 3, Supporting Information Table S3). In general, concentrations of both isotopes are similar to those reported in previous years at this location (Hayes et al. 2015). Activities of ^{230}Th, produced at a near-constant rate from the decay of ^{234}U, were invariant in the upper 100 m at ~ 0.45 μBq kg^{-1} (2.7 aM), and increased linearly below this depth (Fig. 3). This is similar to values of 0.6 μBq kg^{-1} measured by Hayes et al. (2015) in July 2012. The stable ^{232}Th isotope derives from dissolution of atmospheric aerosols and peaked in the mixed layer (47 fM), within the 20–100 fM range of prior measurements. If it is assumed that ^{232}Th and ^{230}Th have identical physiochemical speciation, their relative removal rates from the upper ocean should be equivalent, even though their sources are distinct. This allows calculation of the dissolved Th residence time based on the production rate and inventory of ^{230}Th, equal to ~ 1.3 yr for a 0–150 m integral that encapsulates the entire primary production zone, as well as the maximum winter mixed layer depth at Station ALOHA (Karl et al. 2021) (*see* also Supporting Information Fig. S2). This residence time can then be used to determine the input rate of ^{232}Th from dust deposition based on its measured inventory (3.73 nmol m^{-2} yr^{-1} when integrated to 150 m; Fig. 3c). Using the 14.6 ppm abundance of ^{232}Th in dust and 5.2% relative Th solubility suggested by Hayes et al. (2013), this implies an annually averaged dust flux of ~ 1.1 g m^{-2} yr^{-1} (or 3 mg m^{-2} d^{-1}). This value is broadly consistent with the measured Al flux, although the Th estimate may be elevated because it integrates across a longer timescale, and therefore records peak dust deposition during spring that has sunk well below our deepest sediment trap. Although the North Hawaiian Ridge Current is expected to shield Station ALOHA from terrigenous input from the Hawaiian Islands (Boyle et al. 2005), we cannot rule

Table 3. Sinking Fe fluxes from PIT sediment traps.

Depth/deployment		Fe flux μmol m^{-2} d^{-1}	Al flux μmol m^{-2} d^{-1}	Fe : Al mol : mol	Non-lithogenic Fe flux μmol m^{-2} d^{-1}
KM1910 Station ALOHA 15 June 2019 to 22 June 2019 (this study)					
75 m	1	2.12 ± 0.12	4.18 ± 049	0.51 ± 0.05	0.95 ± 0.11
	2	2.71 ± 0.78	4.83 ± 0.82	0.56 ± 0.09	1.36 ± 0.59
150 m	1	1.88 ± 0.20	4.15 ± 0.73	0.46 ± 0.09	0.72 ± 0.25
	2	2.53 ± 0.49	3.93 ± 0.41	0.66 ± 0.18	1.43 ± 0.59
300 m	1	3.04 ± 0.54	7.27 ± 0.61	0.42 ± 0.11	1.00 ± 0.71
	2	2.33 ± 0.67	5.25 ± 0.34	0.44 ± 0.13	0.86 ± 0.66
VERTIGO Station ALOHA 22 June 2004 to 08 July 2004 (Lamborg et al. 2008)					
150 m		4.0 ± 1.6	8.7 ± 4.5	0.52 ± 0.25	1.55 ± 1.40
300 m		3.9 ± 1.8	10.8 ± 5.7	0.39 ± 0.08	0.90 ± 0.88

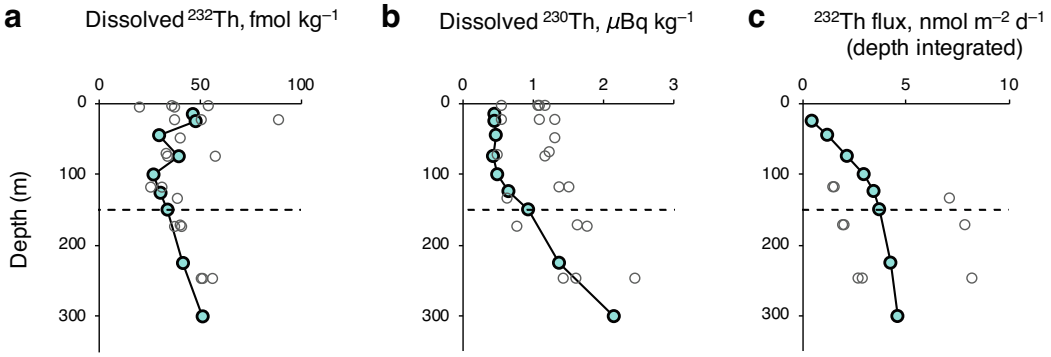

Fig. 3. Thorium isotope distributions at Station ALOHA. Profiles of ^{232}Th (**a**), ^{230}Th (**b**), and the inferred flux of ^{232}Th (**c**), derived as per Hayes et al. (2013). Observations from June 2019 are plotted in cyan. Gray circles indicate past measurements at Station ALOHA reported by Hayes et al. (2015). The dashed line at 150 m highlights the integration depth used for mass balance calculations, *see* "Results" section.

out the possibility that the higher Th-derived flux also reflects island sources of ^{232}Th and Fe to this region, in addition to atmospheric deposition.

The analogous source flux of dFe can be estimated if it is assumed that Fe and dust-derived ^{232}Th have similar relative solubilities (regardless of their absolute value). Following Hayes et al. (2015), we estimate a dFe flux of 41 μmol m^{-2} yr^{-1} (0.11 μmol m^{-2} d^{-1}) by the Th method, with an uncertainty of ~ 50%, largely based on the equal solubility assumption. Note that this represents a flux of Fe to the dissolved phase, and cannot be straightforwardly compared to the Fe flux measured in sediment traps.

Discussion

Biological turnover of dissolved iron in the euphotic zone

The profile of dFe uptake measured at Station ALOHA showed similar rates of 30–50 pM d^{-1} across the upper 125 m (Fig. 1). No significant difference ($p > 0.05$; one way ANOVA) was identified across the depth profile, despite a > 5-fold difference in dFe between the mixed layer and the lower euphotic zone. Arriving at these bulk uptake rates requires an extrapolation from the turnover time of the added Fe_{DS} (i.e., Equation 3) to the entire pool of dFe (Eq. 4), which may not be entirely correct. Equilibration of added metals with the natural ligand pool can be a slow process, and is thought to be initiated by binding of inorganic Fe species with weaker organic ligands, followed by subsequent exchange with progressively stronger ligands (Hering and Morel 1989; Hassler et al. 2011). If kinetically slow ligands comprise the majority of the Fe ligand pool, extrapolated bulk uptake rates would overestimate true uptake fluxes. Although this concern cannot be entirely addressed here, by conducting preincubations over timescales similar to those required for the determination of organic ligands by voltammetry, it can be inferred that Fe added to the incubation is bound by relatively strong ligands with similar characteristics to those previously observed at

Station ALOHA (500–1000 pM, log $K_{Fe',app}$ = 11 – 12.5; Fitzsimmons et al. 2015*b*; Bundy et al. 2018).

But, given the presence of an excess pool of strong ligands, is an Fe uptake rate of 50 pM d^{-1} even possible? Similar Fe uptake rates have also been reported in HNLC environments in the Equatorial Pacific (Price et al. 1994), Subarctic Pacific (Schmidt and Hutchins 1999), and Southern Ocean (Ellwood et al. 2020) using radiotracers but biomass and productivity in these regions are generally greater and Fe is sometimes artificially high due to incubation conditions. Below we consider the potential for Fe′ uptake, which is universally bioavailable. If an estimated 500 pM of excess, uncomplexed ligands in the mixed layer (dFe = 445 pM) is assumed to have a binding strength of $10^{11.5}$ M^{-1}, Fe′ at equilibrium should be ~ 2.8 pM. Based on this quantity, the maximum diffusive flux to a particle and/or cell surface can be calculated according to:

$$\rho_{Fe'} = 4\pi RD[Fe'][\text{particles L}^{-1}], \quad (5)$$

where D is the diffusivity of Fe′ in seawater, 9×10^{-6} cm^{-2} s^{-1}, and R is the radius of the cell or particle (Hudson and Morel 1990). Primary production throughout the water column at Station ALOHA is dominated by *Prochlorococcus* (Rii et al. 2016). Applying a cell radius of 0.3 μm and an abundance of 200,000 cells mL^{-1} measured in June 2019 (Fig. 1b), the diffusive flux of Fe′ to the cell surface of *Prochlorococcus* would be 165 pM d^{-1} (Fig. 4). Based on the abundance of heterotrophic bacteria (~ 500,000 cells mL^{-1}) and assuming R = 0.2 μm, an even greater maximum uptake rate could be expected (~ 275 pM d^{-1}). This suggests that the small size and abundance of autotrophic and heterotrophic bacteria at ALOHA could account for the observed uptake based on Fe′ alone.

Diffusion places stronger constraints on the ability of larger organisms to contribute to uptake of Fe′ (Fig. 4a). Only 4.7 pM d^{-1} Fe′ will reach the 860 cell mL^{-1} population of picoeukaryotes (assuming a 2 μm radius), and less than 2 pM d^{-1} Fe′ will reach *Synechococcus* (1200 cell mL^{-1}, 0.5 μm), *Crocosphaera* (estimated to be < 200 cell ml^{-1}, 2.5 μm based on Wilson et al. 2017), and other low abundance diazotrophs like *Trichodesmium* and *Richelia* (typically < 10 cell mL^{-1}; White et al. 2018). Although removal of Fe′ onto lithogenic particles has been emphasized during dust storms in the Equatorial Atlantic (Ye and Völker 2017), it appears unlikely that this is significant at Station ALOHA, at least during the summer. For instance, if it is assumed that the measured particulate Al concentration in the mixed layer (0.23 nM) reflects crustal aluminosilicates (8% Al by weight, 4 g cm^{-3}), scavenging of Fe′ onto the surface of these particles—580 dust particles mL^{-1} at a 0.2 μm radius—must also be < 1 pM d^{-1}.

Overall, uptake rates on the order of 30–50 pM d^{-1} can be rationalized if ~ 10% of the diffusive flux of Fe′ to cell surfaces is acquired, but only to *Prochlorococcus*, heterotrophic bacteria, and perhaps adsorption onto nonliving organic detritus (estimated at 60–70% of particulate matter at Station ALOHA; Henderikx-Freitas et al. 2021). For this mechanism to be valid, Fe′ must be replaced through dissociation of FeL complexes. Assuming that FeL dissociation constants reported for the North Atlantic and Arabian Sea apply here ($k_d \geq 2 \times 10^{-6}$ s^{-1}; Witter and Luther III 1998; Witter et al. 2000), Fe′ replacement rates could be > 75 pM d^{-1}, enough to balance Fe uptake. This rate is likely much greater during daytime in the mixed layer due to photochemical generation of Fe′ from FeL complexes (Fan 2008; Shaked et al. 2020).

Observed Fe uptake rates can also be rationalized by comparison to recent measurements of *Prochlorococcus* Fe requirements. Most *Prochlorococcus* in surface waters at Station ALOHA belong to the HLII ecotype and culture experiments with the HLII *Prochlorococcus* strain MIT9215 suggest the onset of Fe limitation at an Fe : C ratio of ~ 11 μmol : mol (Hawco et al. 2020*a*). If all of the gross primary production at ALOHA is performed by *Prochlorococcus* (or by organisms with similar Fe requirements), then the 1.1 μM O_2 d^{-1} measured in the mixed layer would require uptake of at least 7.3 pM Fe d^{-1} (using a ratio of 1.7 to convert GOP to net C uptake; Ferrón et al. 2016; Fig. 1b). The metabolic state of the oligotrophic ocean is only weakly autotrophic, with heterotrophic respiration largely balancing net primary production (Ferrón et al. 2021). At a heterotrophic Fe : C ratio of 8 μmol : mol and a bacterial growth efficiency of 0.26 (Tortell et al. 1996), consuming the net O_2 produced by *Prochlorococcus* and other phytoplankton could increase this minimum Fe demand by a further 1.4 pM Fe d^{-1}. It should be noted that Fe requirements for *Pelagibacter* (SAR11) and other abundant heterotrophs at Station ALOHA have not yet been characterized so there is a large uncertainty associated with this Fe : C value. Regardless, the 35 pM d^{-1} Fe uptake in the mixed layer—equivalent to an Fe : C uptake ratio of ~ 50 μmol : mol—corresponds to a 4-fold excess over this estimated Fe limitation threshold. Uptake not associated with primary production (e.g., by adsorption onto organic detritus) would detract from this excess and perhaps push *Prochlorococcus* closer to Fe limitation. The mixed layer Fe : C uptake ratio (Fig. 1f) still falls below the expected maximum *Prochlorococcus* quota (100–200 μmol : mol; Hawco et al. 2021*b*; Shire and Kustka 2015), implying that Fe uptake is not saturated and would continue to increase with increasing dFe.

Deeper in the water column, growth at lower light conditions is expected to require greater Fe : C biomass ratios due to upregulation of the photosynthetic apparatus (Raven 1990). In culture experiments under DCM conditions, the transition to Fe-limited growth in the *Prochlorococcus* MIT1214 strain, an LL1 ecotype isolated from the lower euphotic zone at Station ALOHA, occurred when the Fe : C ratio fell below ~ 30 μmol : mol (Hawco et al. 2021*b*). Based on mean O_2 production at 100 m (0.32 μM d^{-1}; Fig. 1a), growth of low-light

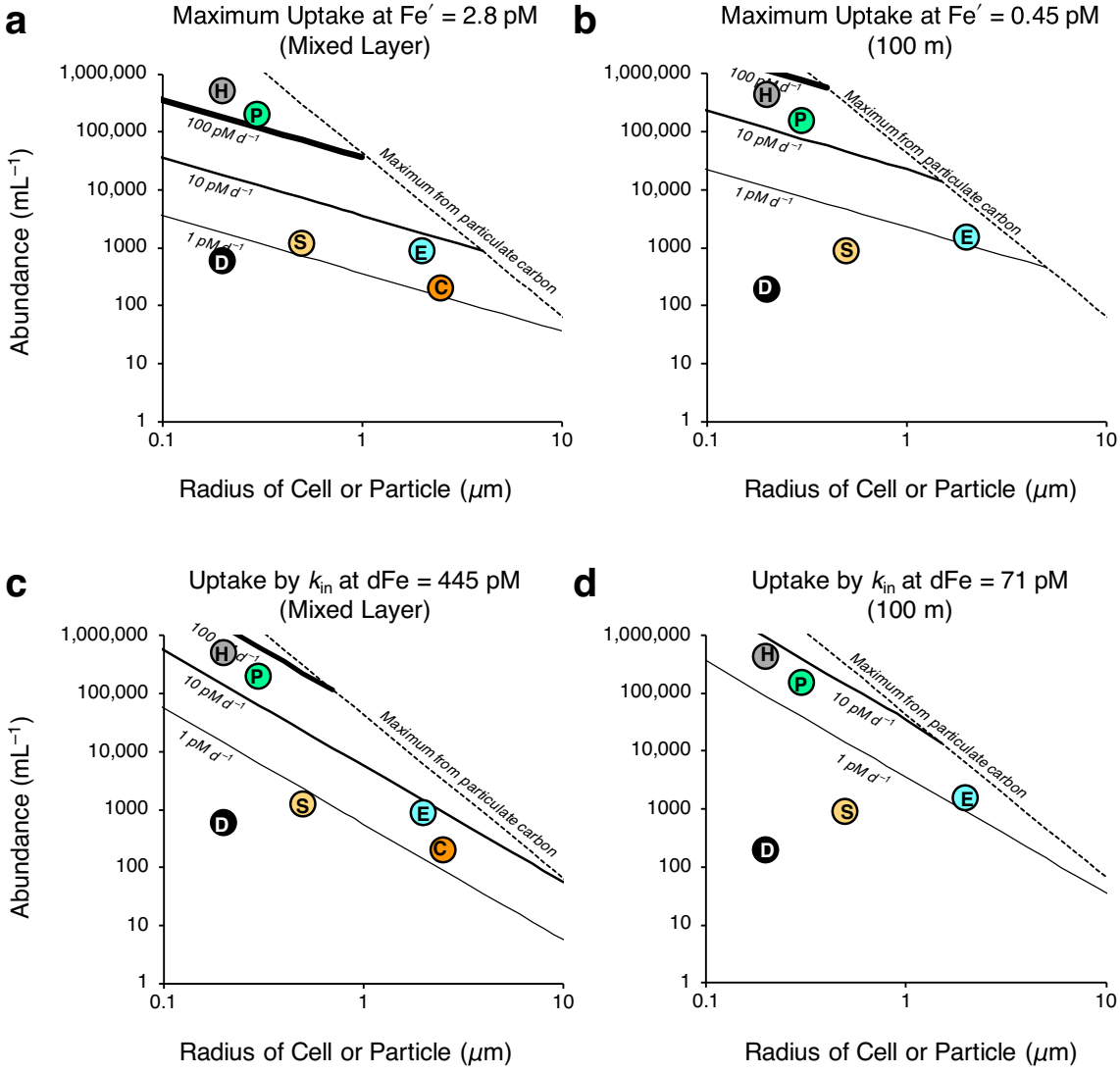

Fig. 4. Kinetic constraints on iron uptake based on the diffusion of unchelated Fe′ (**a**,**b**) or apparent internalization constants, k_{in}, applied to dFe (**c**,**d**). Maximum Fe′ uptake rates in the mixed layer (**a**) and at 100 m (**b**) are calculated by Eq. 5, with estimated radii of *Prochlorococcus* (P, 0.3 μm), heterotrophic bacteria (H, 0.2 μm), Picoeukaryotes (E, 2 μm), *Synechococcus* (S, 0.5 μm), *Crocosphaera* (2.5 μm), and lithogenic dust (D, 0.2 μm). Abundances reflect flow cytometry measurements except for *Crocosphaera* (estimated from Wilson et al. 2017) and dust (from particulate Al). The surface area normalized k_{in} value of 3.16×10^{-10} L μm^{-2} d^{-1} originates from Shaked et al. (2021). Constraints from an upper limit of a representative concentration of 3 μM particulate carbon is estimated using C : biovolume power law relationship of Menden-Deuer and Lessard (2000) derived for all phytoplankton except diatoms.

adapted *Prochlorococcus* probably required Fe uptake of at least 5.6 pM d^{-1} to avoid Fe limitation. Lower net productivity at 100 m implies that heterotrophic Fe demand may be lower than in the surface (0.4 pM d^{-1}). In the lower euphotic zone, Fe uptake from Fe′ diffusion would only allow a maximum Fe′ flux of 20 pM d^{-1} to *Prochlorococcus* cells, assuming an abundance of 150,000 cells mL^{-1} (there is some uncertainty due to vertical oscillations in the lower euphotic zone between casts; Supporting Information Fig. S3; *see* also Letelier et al. 1993). Instead, it is likely that much of the *Prochlorococcus* Fe uptake in the lower euphotic zone is driven by uptake of FeL complexes, which is supported by new genomic evidence for siderophore acquisition in LL1 *Prochlorococcus* in the lower euphotic at Station ALOHA (Hogle et al. 2022). The fast turnover time of pre-equilibrated Fe_{DS} in the lower euphotic zone (1.4–2.5 d, which approaches the timescale of the incubation) provides additional evidence that the FeL pool is bioavailable.

Observations with phytoplankton in culture have shown that actual Fe uptake rates rarely approach the diffusion maximum because coordination reactions with Fe transporters can be rate limiting. The kinetics of transporter binding can be quantified by k_{in} (units: L cell^{-1} d^{-1}), a clearance rate

parameter that, when multiplied by a bioavailable Fe concentration, yields an Fe uptake rate. Shaked et al. (2021) have recently derived a scaling relationship between k_{in} and cell surface area for wild eukaryotic phytoplankton based on single cell Fe : C measurements in Fe-limited regions. When scaled to the abundance and approximate size of picoeukaryotes at ALOHA, this yields a k_{in} of 1.6×10^{-8} L cell^{-1} d^{-1} and an estimated Fe uptake of 6.1 pM d^{-1} in the mixed layer and 1.7 pM d^{-1} at 100 m (Fig. 4c,d). There is no field-based estimate of k_{in} for *Prochlorococcus*, but this parameter can be derived from Fe-limited culture experiments by dividing measured Fe uptake rates by Fe′. For the high-light adapted MIT9215 strain (Hawco et al. 2020*a*), k_{in} averages $7.0 \pm 1.5 \times 10^{-10}$ L cell^{-1} d^{-1}, which is similar to the k_{in} of $6.6 \pm 2.2 \times 10^{-10}$ L cell^{-1} d^{-1} for the low-light-adapted MIT1214 strain (Hawco et al. 2021*b*). This suggests that the same Fe transporter is used by both strains and is within a factor of 2 of the extrapolated eukaryotic k_{in} from Shaked et al. (2021) when scaled to a cell with a 0.3 μm radius (3.6×10^{-10} L cell^{-1} d^{-1}). The mean of the *Prochlorococcus* k_{in} estimates (6.8×10^{-10} L cell^{-1} d^{-1}) predicts *Prochlorococcus* Fe uptake of 60 pM Fe d^{-1} in the mixed layer. Note that this calculation represents a maximum case where all dFe is bioavailable (similar calculations with Fe′ lead to implausibly low uptake rates, < 1 pM d^{-1}). At 100 m, the predicted maximum of 7.2 pM d^{-1} from k_{in} is very close to the predicted minimum of 5.6 pM d^{-1} based on the Fe limitation threshold. This can only be achieved if Fe transporters are maximally upregulated and nearly all dFe is bioavailable. As a result, the very high Fe : C uptake ratio inferred from the Fe_{DS} uptake incubations at 100 m (188 ± 42 μmol : mol; Fig. 1f) likely does not reflect the nutritional status of *Prochlorococcus* in the DCM, unless these organisms possess an alternate, unidentified transporter with much greater affinity than the cultured representatives examined thus far. Meanwhile, the k_{in} of marine heterotrophic bacteria remains unconstrained, but rationalizing measured uptake rates at 100 m would seem to require values of the same magnitude as *Prochlorococcus* and eukaryotic phytoplankton. A significant contribution by abiotic adsorption of Fe onto particle surfaces could also explain the high Fe : C uptake ratios in the DCM, but this would seem to require the presence of "dead" Fe transporters, or other equally high-affinity binding sites within the pool of non-living particulate matter.

Timescales of Fe turnover at Station ALOHA

Prior seasonally resolved observations at Station ALOHA are consistent with peak dFe during spring, when atmospheric supply of Asian dust is most intense (Prospero et al. 2003; Boyle et al. 2005; Hyslop et al. 2013). In summertime, however, dFe appears relatively steady, with surface concentrations of 310 ± 140 pM decreasing to 65 ± 22 pM between 90 and 125 m (Fitzsimmons et al. 2015*b*). Below the euphotic zone, concentrations increase through the mesopelagic, in concert with nitrate and other regenerated nutrients. Based on Th isotope measurements at Station ALOHA, Hayes et al. (2015) suggested a dissolved Fe residence time on the order of 6–12 months for the euphotic zone as a whole, which is consistent with strong seasonality in Fe supply due to atmospheric deposit of desert dust.

In general, the inventories of Fe measured during June 2019 were similar to those observed at this location in previous years. dFe concentrations in the mixed layer, 436 ± 19 pM for 0–25 m samples, were within the range reported from previous measurements, as were tdFe concentrations from unfiltered samples: 651 ± 54 pM (Station ALOHA tdFe mean: 760 ± 440 pM; Boyle et al. 2005; Fitzsimmons et al. 2015*a*,*b*). Both dFe and tdFe profiles indicated minimum concentrations at 100 m (Fig. 1c). Based on these measurements, the dFe inventory in the upper 150 m is calculated to be 29.4 ± 1.7 μmol Fe m^{-2}. The corresponding tdFe inventory was 63.6 ± 2.3 μmol Fe m^{-2}. The difference between these pools, 34.2 ± 2.8 μmol Fe m^{-2}, reflects a labile particulate inventory (labile pFe) that presumably encompasses biological Fe phases, reactive components of dust, and Fe scavenged from the water column. Although there is uncertainty over what biological and/or mineralogical phases the labile pFe pool encompasses, the mean labile pFe concentration over 0–150 m of 220 pM agrees with the concentrations of non-lithogenic particulate Fe collected from large volume pumps at 25 and 100 m depth (195 and 202 pM, respectively, calculated by Al correction as for sediment trap samples; Supporting Information Table S2). Thus, we consider the operationally defined quantities of labile pFe and non-lithogenic pFe to be equivalent and interchangeable, at least for the scope of this study. The flux of both lithogenic and non-lithogenic Fe observed in June 2019 are also similar to that observed by Lamborg et al. (2008) during June and July 2004 (*see* Table 3). While our dataset is unique in that inventories and fluxes were documented over the same time period, broad agreement with previous work suggests that the Fe cycle at Station ALOHA is in a near-steady state.

For the upper euphotic zone (0–75 m, the depth of the first sediment trap), comparing the inventory of labile pFe to the non-lithogenic Fe flux in sediment traps at 75 m (1.15 ± 0.30 μmol m^{-2} d^{-1}) yields a residence time of 16 ± 5 d with respect to the sinking flux (τ_{sink}; Fig. 5). A separate "turnover time" of 6.5 ± 2.3 d is derived relative to the measured uptake rates (τ_{up}). This suggests that the labile pFe pool is recycled 2.5 times, on average, before it sinks out of the upper euphotic zone, yielding a combined replacement timescale of 4.6 ± 1.3 d for labile pFe. Calculations for the lower euphotic zone are similar, but indicate a somewhat faster timescale (3.1 ± 0.6 d). It is important to recognize that these descriptions depend on the assumption that the entire labile pFe pool is equally accessible to ecosystem recycling processes. If, for instance, the sinking flux of non-lithogenic Fe is dominated by undissolved dust, a smaller pool of biogenic pFe must turn

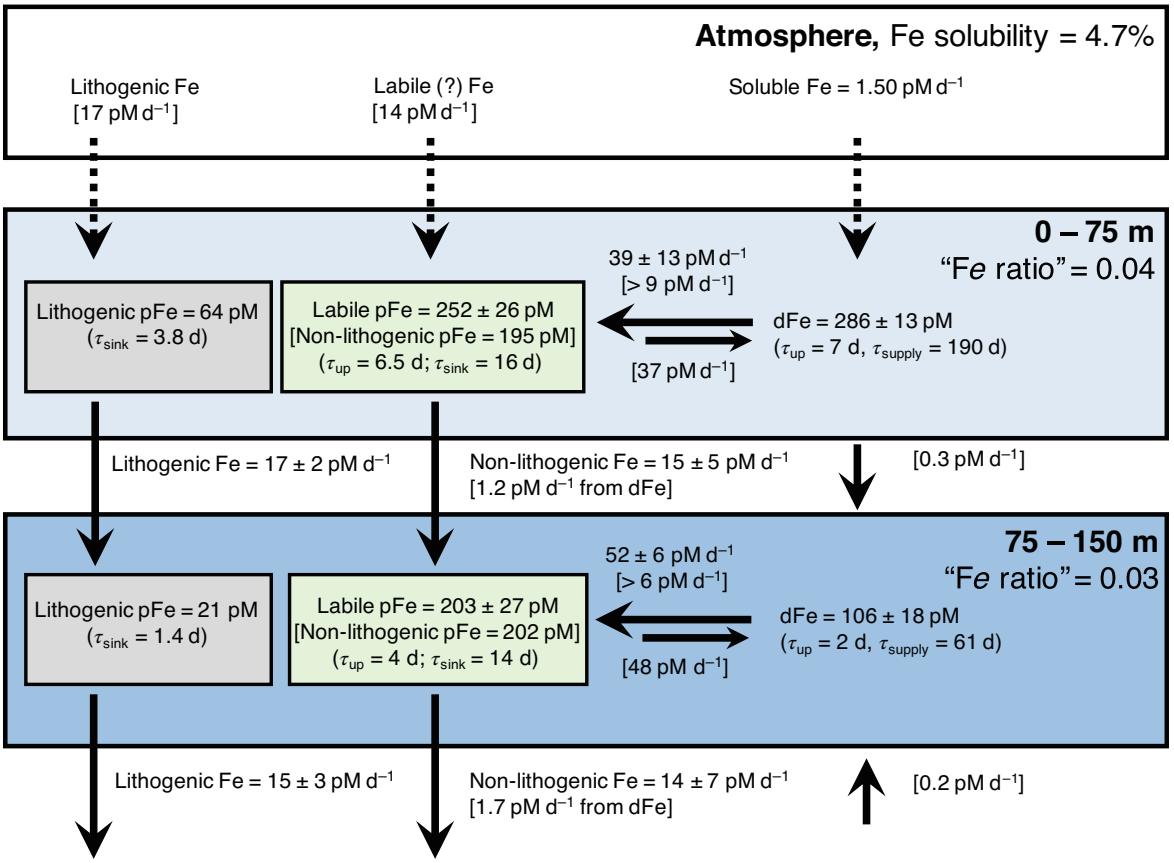

Fig. 5. Station ALOHA iron budget for June 2019. Fe cycling timescales (τ) are derived with respect to uptake (τ_{up}), export (τ_{sink}), or supply (τ_{supply}). Dissolved iron (dFe) is taken up into labile particulate Fe (pFe), which reflects Fe associated with a variety of living and nonliving particles. Labile pFe is either recycled back to dFe or sinks into the lower euphotic zone (75–150 m). Labile pFe derives from the difference between measured tdFe and dFe. Lithogenic pFe is calculated from measured pAl and a stoichiometry of 0.28 mol Fe : mol Al for Asian dust (Arimoto et al. 2004; Buck et al. 2006). An estimate of the non-lithogenic pFe concentration is obtained from pFe minus lithogenic Fe, in brackets. Sinking fluxes of lithogenic Fe and non-lithogenic Fe are calculated analogously. Lithogenic and labile pFe are replaced by atmospheric deposition, along with a directly soluble flux, based on the Th isotope mass balance. Mixing fluxes are derived from vertical dFe gradients, assuming a representative vertical diffusivity of 10^{-4} m^2 s^{-1}. Other bracketed quantities are inferred assuming steady state. Minimum Fe uptake rates in brackets are calculated based on minimum requirements for high- and low-light adapted *Prochlorococcus* ecotypes, as well as heterotrophic bacteria (*see* "Discussion" section; Fig. 1d).

over more frequently to arrive at the mean turnover times calculated above.

The mean turnover time of dFe with respect to uptake (τ_{up}) over the 0–75 m interval is 7.4 ± 2.5 d. Broadly speaking, the dFe pool in the upper euphotic zone is recycled once per week. The same caveat regarding accessibility of the labile pFe pool during remineralization could also be applied for dFe uptake; indeed, it is not established how quickly dFe in the colloidal size range (> 10 kDa) exchanges with smaller size (so-called "soluble") dFe, which includes both very strong organic ligands like siderophores and bioavailable Fe′ (Fitzsimmons et al. 2015*a*). While each of these pools likely cycle at distinct rates, there must be a limit to this heterogeneity: to meet growth requirements, the productivity-scaling calculations suggest that *Prochlorococcus* must be able to access at least 10% of the dFe pool in the mixed layer (based on k_{in}), and likely more if cells are comfortably replete in Fe and Fe transporters are not maximally upregulated.

Ecosystem recycling at ALOHA leads to the replacement timescale for dFe, or the residence time with respect to external sources (τ_{supply}), being considerably longer than the uptake-derived turnover time. Estimating this flux requires a constraint on the external input of dFe, which can be generated from dissolved Th isotopes. If it is assumed that both the Fe and ^{232}Th supplied from dust dissolve to equal extents in the upper ocean, the measured 0–150 inventories of ^{230}Th and ^{232}Th indicate a flux of 0.11 μmol Fe m^{-2} d^{-1}, or 1.5 pM d^{-1} added to the upper euphotic zone (0–75 m, note that the ~ 1 yr residence time of Th requires an integration to below the maximum winter mixed layer). Using the Th-derived flux, the dFe residence time for the upper euphotic zone is calculated to be 190 ± 95 d, roughly 6 months. Relative to the total

Fe flux recorded in sediment traps (2.4 μmol m^{-2} d^{-1}), the Th-derived flux implies an aerosol Fe solubility on the order of 4.7% ± 2.6%. Although the timescales governing the Th-derived and sediment trap fluxes are distinct, it is encouraging that campaigns to sample aerosols in the Western North Pacific during spring have observed both elevated Fe : Al ratios averaging 0.53 mol mol^{-1} (our sediment traps record Fe : Al ranging 0.43–0.55) and aerosol Fe solubilities on the order of 6% ± 5% in seawater (Buck et al. 2006).

To complete the 0–75 m budget, the effect of diffusive mixing must also be acknowledged. The steep gradients in dFe in the upper 150 m indicate a net export of dFe from the upper to the lower euphotic zone. While vertical diffusivity in the upper ocean is subject to order-of-magnitude level uncertainty and dominated by episodic events that often escape observation (Johnson et al. 2010), applying a relatively large diffusivity value of 10^{-4} m^2 s^{-1} (Keeling et al. 2004) to the gradient in dFe leads to a removal flux of ~ 0.3 pM d^{-1}. Although constraints on the diffusive Fe flux are weak at this stage, they are required for steady-state estimates of both the remineralization flux of dFe (37 pM d^{-1}) and the export of dFe below 75 m via the biological pump (1.2 pM d^{-1}). The short apparent turnover time of labile pFe should add confidence that the steady state assumption is reasonable over timescales of a few weeks. We expect the remineralization flux driving pFe turnover is mostly influenced by protistan grazers, which appear to be responsible for the majority of *Prochlorococcus* mortality at Station ALOHA (Frias-Lopez et al. 2009; Mruwat et al. 2021).

Continuing the steady-state assumption allows for a parallel budget for the lower euphotic zone (Fig. 5). Here, the combined supply of ~ 1.5 pM d^{-1} of Fe from export and mixing is further supplemented by the upward diffusion of dFe from the nutricline of an additional ~ 0.2 pM d^{-1}. The estimated residence time is 61 ± 32 d (τ_{supply}), whereas the recycling timescale appears to be on the order of 2 d. As a whole, the 0–150 m euphotic zone has a dFe residence time of 236 ± 119 d, roughly 8 months. It should be noted that this 1D budget ignores advective inputs of either dFe or pFe from the Hawaiian Islands, whose significance at Station ALOHA is currently unresolved.

Boyd et al. (2005) introduced the concept of the "F*e* ratio," being the ratio of Fe export rates to Fe uptake rates. Like the classical *e*- and *ef*-ratios used to describe the fraction of primary production or nitrogen uptake that is exported below the euphotic zone (Murray et al. 1989; Karl et al. 1996), the F*e* ratio serves as an indicator of an ecosystem's ability to retain Fe in the euphotic zone to fuel primary production (Boyd et al. 2005). Accordingly, F*e* ratios below 0.1 imply that the average Fe atom is recycled > 10 times before export. Low F*e* ratios (< 0.1) are associated with Fe-limited regions such as the Equatorial Pacific and the open waters of the Southern Ocean (Boyd et al. 2005; Rafter et al. 2017; Ellwood et al. 2020). In contrast, Fe replete ecosystems should have high F*e* ratios because of an excess in new Fe supply, as observed in naturally fertilized areas of the Southern Ocean (Chever et al. 2010; Bowie et al. 2015). Based on this conceptual understanding, Station ALOHA has been proposed to operate at a high F*e* ratio (Boyd et al. 2017), but concurrent measurements of Fe uptake or export were not available then.

The June 2019 Fe budget at Station ALOHA leads to calculation of very low F*e* ratios for both the upper and lower segments of the euphotic zone (Fig. 5). For the 0–75 m interval, the F*e* ratio is calculated to be 0.04 (= 1.5 pM d^{-1} dFe supply ÷ 39 pM d^{-1} dFe uptake) with a similar value of 0.03 also determined for the 75–150 m interval. For both depth ranges, this implies that the average Fe atom experiences 25–30 uptake and recycling episodes prior to export. Treated as a whole, the 0–150 m euphotic zone bears an F*e* ratio of 0.02, which is perhaps even lower than the long-term *e*-ratio at Station ALOHA of 0.054 (Karl et al. 2021).

Like the *e*-ratio, the original calculations of the F*e* ratio during the FeCycle campaign used sediment trap-derived Fe fluxes to infer the input of new Fe to the euphotic zone. If our 150 m sediment trap fluxes of non-lithogenic Fe are used to derive the F*e* ratio (instead of the Th-derived Fe supply), then a much higher value of 0.16 is calculated for 0–150 m (Fig. 6), which is near the F*e* ratio of 0.09 determined in the Subantarctic during FeCycle (Boyd et al. 2005). This value would describe a very different state of Fe recycling (6 revolution of the microbial "ferrous wheel") and so it is worth considering the assumptions that underlie both of these calculations. The high F*e* ratio scenario is driven by a greater export flux of Fe, defined by the non-lithogenic component within the sediment trap, and assumes that this quantity originated from the dFe pool. In principle, this appears plausible because the labile pFe recycling timescale is much shorter than the export timescale (i.e., $\tau_{up} \ll \tau_{sink}$; Fig. 5). In order to achieve a steady state, however, less compelling aspects of this high F*e* ratio framework emerge (Fig. 6b). For one, the required solubility of aerosol Fe must be on the order of 48%, which exceeds that found in most dissolution experiments. Aerosol Fe solubilities > 20% have been observed when acidic and reducing leaches are applied (Shelley et al. 2018), but this would seem to require more involved solubilization processes, for example, ingestion by zooplankton and solubilization in anoxic and acidic digestive tracts. Given the low quantities of dust relative to other particulate pools at Station ALOHA (Fig. 4), it is unclear if most dust-derived particles are ingested by zooplankton or protistan grazers prior to export. Furthermore, the elevated F*e* ratio scenario in Fig. 6b requires a substantially shorter dFe residence time (27 d) that implies either much lower dFe inventories once the springtime pulse of Asian dust fades away or a major role for anthropogenic or biomass-burning aerosol Fe supply to continue supplying Fe during summer and fall (without supplying Th). Although there is evidence that anthropogenic Fe can be a significant supply term (Conway

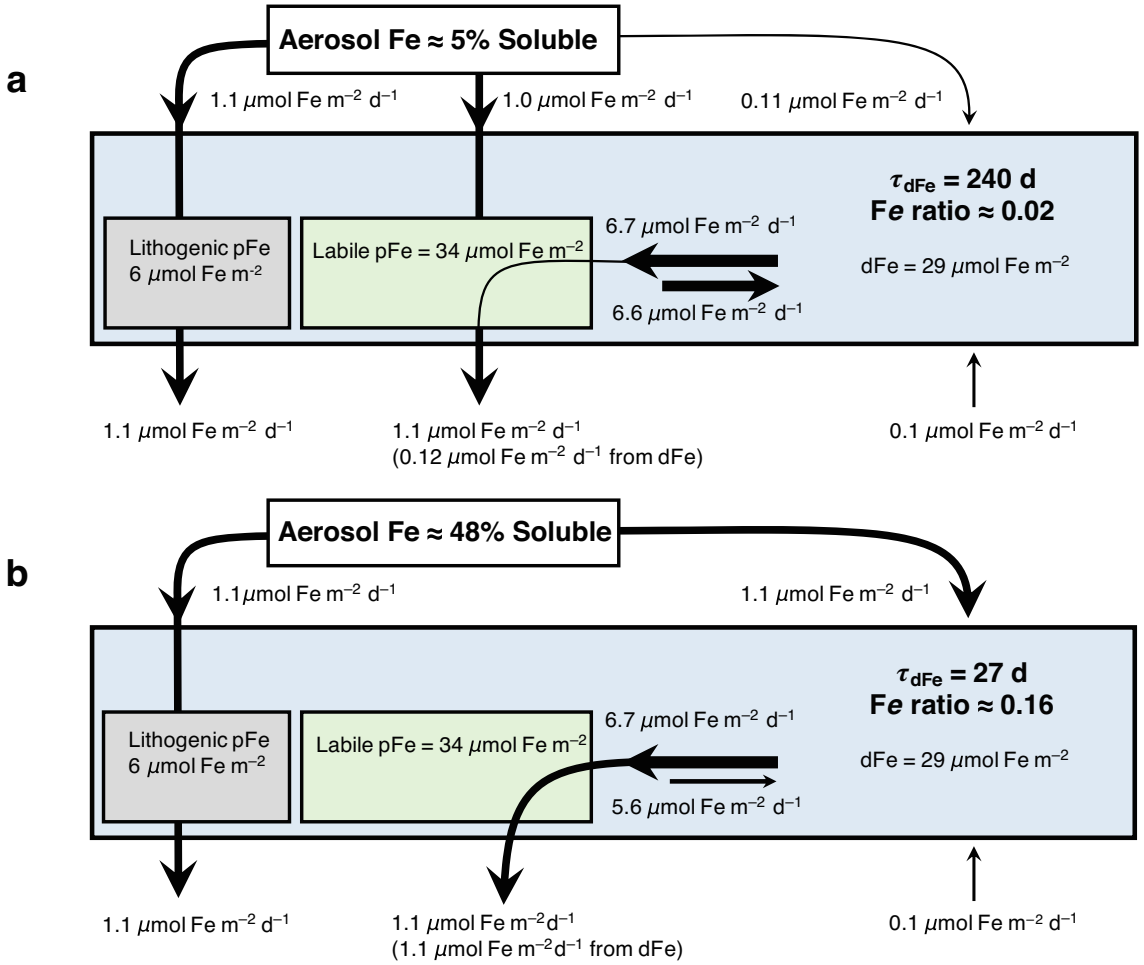

Fig. 6. Comparison of two Fe cycling scenarios for the euphotic zone at Station ALOHA (0–150 m). (**a**) A moderate solubility scenario where most (90%) of the non-lithogenic Fe flux measured in sediment traps derives directly from aerosols and the remainder (10%) derives from dFe uptake onto particles. This leads to a low F*e* ratio and a ~ 8-month residence time of dFe. (**b**) A very high-solubility scenario where all non-lithogenic Fe passes through the dissolved phase, producing a more moderate F*e* ratio (0.16) but monthly replacement of the dFe pool.

et al. 2019; Ito et al. 2019; Pinedo-González et al. 2020), it does not seem likely to account for most of the dFe supply to Station ALOHA. Furthermore, summertime observations of dFe have shown steady and moderate concentrations from June to September (Fitzsimmons et al. 2015*b*), suggesting a considerably longer residence time applies.

Instead, the lower F*e* ratio advocated by Th supply points to a more reasonable explanation of our results: that only a fraction of the chemically labile or non-lithogenic Fe supplied from the atmosphere will actually exchange with dFe before it sinks out of the euphotic zone. If these low F*e* ratios are correct, it suggests that oligotrophic ecosystems have an underappreciated capacity to retain dFe in the euphotic zone, even if the lack of Fe-limiting conditions at Station ALOHA means that there may be little physiological incentives to do so. It may be that imperatives to recycle scarce macronutrients (e.g., NH_4^+, PO_4) that drive low *e*-ratios in the subtropical North Pacific also result in the recycling of dFe as well. This would imply that ecosystems that are replete in both macronutrients and Fe would have the lowest Fe recycling efficiency, which is broadly consistent with the high F*e* ratios found in naturally fertilized regions of the Kerguelan Plateau or off the coast of New Zealand during FeCycle II (Chever et al. 2010; Bowie et al. 2015; Boyd et al. 2015). This "inherent" recyclability of Fe in oligotrophic settings could help explain how phytoplankton in other oligotrophic regions like the South Pacific Gyre can remain predominantly nitrogen limited (Bonnet et al. 2008), despite receiving a much lower flux of Fe from the atmosphere.

Conclusions

The application of MC-ICPMS for tracer studies has the potential to constrain uncertainty in the iron cycle. Addition of a few pM of isotope spike allows for precise measurements of Fe uptake rates throughout the euphotic zone. Other

applications of this approach could include the kinetics of Fe binding and exchange to siderophores and organic ligands, cycling of colloidal Fe, or partitioning of acquired Fe between and within cells, or among nonliving particles. Similar versions of these experiments can also be developed for other micronutrient metal isotope systems (e.g., Cu, Ni, Zn, Cd).

The Fe uptake rates at Station ALOHA point toward an ecosystem that is highly dependent on Fe recycling. The dFe inventory in the upper euphotic zone recycles on weekly timescales and is replaced over a timescale of ~ 6 months, likely experiencing over a dozen revolutions before being exported. However, we cannot fully rule out a less efficient Fe cycle maintained by a large supply of anthropogenic Fe. While it seems unlikely at this stage, if this latter scenario is true—an idea originally asserted for this region by Boyle et al. (2005)—then the apparent surplus Fe uptake by *Prochlorococcus* and heterotrophs revealed by our experiments (4-fold greater than estimated minimum requirements) might also be an artifact of the Anthropocene Ocean. More generally, uncertainties in aerosol Fe supply and ecosystem recycling appear to compensate for each other and it will be difficult to determine the correct magnitude of soluble Fe supply in biogeochemical models if Fe recycling processes are unconstrained (or vice versa). Observations that differentiate between the spectrum of possible high recycling/low solubility and low recycling/high solubility scenarios will be needed to evaluate human impacts on the iron cycle and ocean biogeochemistry.

Data availability statement

All data generated for this study can be found in tables in the main text and in the supplementary information. Additional datasets related to the KM1910 project can be found in the Biological and Chemical Oceanography Data Management Office (BCO-DMO), under project number 805876.

References

Arimoto, R., and others. 2004. Chemical composition of atmospheric aerosols from Zhenbeitai, China, and Gosan, South Korea, during ACE-Asia. J. Geophys. Res. Atmos.: **109**: D19S04. doi:10.1029/2004GB002227

Black, E. E., K. O. Buesseler, S. M. Pike, and P. J. Lam. 2018. ^{234}Th as a tracer of particulate export and remineralization in the southeastern tropical Pacific. Mar. Chem. **201**: 35–50.

Bonnet, S., and others. 2008. Nutrient limitation of primary productivity in the Southeast Pacific (BIOSOPE cruise). Biogeosciences. **5**: 215–225. doi:10.5194/bg-5-215-2008

Bowie, A. R., and others. 2015. Iron budgets for three distinct biogeochemical sites around the Kerguelen Archipelago (Southern Ocean) during the natural fertilisation study, KEOPS-2. Biogeosciences **12**: 4421–4445.

Boyd, P. W., and others. 2005. FeCycle: Attempting an iron biogeochemical budget from a mesoscale SF6 tracer experiment in unperturbed low iron waters. Global Biogeochem. Cycl. **19**: GB4S20. doi:10.1029/2004GB002227

Boyd, P. W., and M. J. Ellwood. 2010. The biogeochemical cycle of iron in the ocean. Nat. Geosci. **3**: 675–682.

Boyd, P. W., R. F. Strzepek, M. J. Ellwood, D. A. Hutchins, S. D. Nodder, B. S. Twining, and S. W. Wilhelm. 2015. Why are biotic iron pools uniform across high- and low-iron pelagic ecosystems? Global Biogeochem. Cycl. **29**: 1028–1043.

Boyd, P. W., M. J. Ellwood, A. Tagliabue, and B. S. Twining. 2017. Biotic and abiotic retention, recycling and remineralization of metals in the ocean. Nat. Geosci. **10**: 167–173.

Boyle, E. A., B. A. Bergquist, R. A. Kayser, and N. Mahowald. 2005. Iron, manganese, and lead at Hawaii Ocean Time-series station ALOHA: Temporal variability and an intermediate water hydrothermal plume. Geochim. Cosmochim. Acta **69**: 933–952.

Buck, C. S., W. M. Landing, J. A. Resing, and G. T. Lebon. 2006. Aerosol iron and aluminum solubility in the northwest Pacific Ocean: Results from the 2002 IOC cruise. Geochem. Geophys. Geosyst. **7**: Q04M07. doi:10.1029/2005GC000977

Bundy, R. M., R. M. Boiteau, C. McLean, K. A. Turk-Kubo, M. R. McIlvin, M. A. Saito, B. A. S. Van Mooy, and D. J. Repeta. 2018. Distinct siderophores contribute to iron cycling in the mesopelagic at station ALOHA. Front. Mar. Sci. **5**: 61.

Chever, F., G. Sarthou, E. Bucciarelli, S. Blain, and A. R. Bowie. 2010. An iron budget during the natural iron fertilisation experiment KEOPS (Kerguelen Islands, Southern Ocean). Biogeosciences **7**: 455–468.

Conway, T. M., A. D. Rosenberg, J. F. Adkins, and S. G. John. 2013. A new method for precise determination of iron, zinc and cadmium stable isotope ratios in seawater by double-spike mass spectrometry. Anal. Chim. Acta **793**: 44–52.

Conway, T. M., and S. G. John. 2014. Quantification of dissolved iron sources to the North Atlantic Ocean. Nature **511**: 212–215.

Conway, T. M., and S. G. John. 2015. The cycling of iron, zinc and cadmium in the North East Pacific Ocean—Insights from stable isotopes. Geochim. Cosmochim. Acta **164**: 262–283.

Conway, T. M., D. S. Hamilton, R. U. Shelley, A. M. Aguilar-Islas, W. M. Landing, N. M. Mahowald, and S. G. John. 2019. Tracing and constraining anthropogenic aerosol iron fluxes to the North Atlantic Ocean using iron isotopes. Nat. Commun. **10**: 1–10.

Ellwood, M. J., R. F. Strzepek, P. G. Strutton, T. W. Trull, M. Fourquez, and P. W. Boyd. 2020. Distinct iron cycling in a Southern Ocean eddy. Nat. Commun. **11**: 1–8.

Fan, S.-M. 2008. Photochemical and biochemical controls on reactive oxygen and iron speciation in the pelagic surface ocean. Mar. Chem. **109**: 152–164.

Ferrón, S., D. A. del Valle, K. M. Björkman, P. D. Quay, M. J. Church, and D. M. Karl. 2016. Application of membrane inlet mass spectrometry to measure aquatic gross primary production by the ^{18}O in vitro method. Limnol. Oceanogr. Methods **14**: 610–622.

Ferrón, S., B. Barone, M. J. Church, A. E. White, and D. M. Karl. 2021. Euphotic zone metabolism in the North Pacific Subtropical Gyre based on oxygen dynamics. Global Biogeochem. Cycles **35**: e2020GB006744.

Fitzsimmons, J. N., R. M. Bundy, S. N. Al-Subiai, K. A. Barbeau, and E. A. Boyle. 2015*a*. The composition of dissolved iron in the dusty surface ocean: An exploration using size-fractionated iron-binding ligands. Mar. Chem. **173**: 125–135.

Fitzsimmons, J. N., C. T. Hayes, S. N. Al-Subiai, R. Zhang, P. L. Morton, R. E. Weisend, F. Ascani, and E. A. Boyle. 2015*b*. Daily to decadal variability of size-fractionated iron and iron-binding ligands at the Hawaii Ocean Time-Series Station ALOHA. Geochim. Cosmochim. Acta **171**: 303–324. doi:10.1016/j.gca.2015.08.012

Frias-Lopez, J., A. Thompson, J. Waldbauer, and S. W. Chisholm. 2009. Use of stable isotope-labelled cells to identify active grazers of picocyanobacteria in ocean surface waters. Environ. Microbiol. **11**: 512–525.

Hassler, C. S., V. Schoemann, C. M. Nichols, E. C. V. Butler, and P. W. Boyd. 2011. Saccharides enhance iron bioavailability to Southern Ocean phytoplankton. Proc. Natl. Acad. Sci. **108**: 1076–1081.

Hatta, M., C. I. Measures, J. Wu, S. Roshan, J. N. Fitzsimmons, P. Sedwick, and P. Morton. 2015. An overview of dissolved Fe and Mn distributions during the 2010–2011 US GEOTRACES North Atlantic cruises: GEOTRACES GA03. Deep Sea Res. Part II Top. Stud. Oceanogr. **116**: 117–129.

Hawco, N. J., M. M. McIlvin, R. M. Bundy, A. Tagliabue, T. J. Goepfert, D. M. Moran, L. Valentin-Alvarado, G. R. DiTullio, and M. A. Saito. 2020*a*. Minimal cobalt metabolism in the marine cyanobacterium *Prochlorococcus*. Proc. Natl. Acad. Sci. **117**: 15740–15747.

Hawco, N. J., and others. 2020*b*. Metal isotope signatures from lava–seawater interaction during the 2018 eruption of K⌧lauea. Geochim. Cosmochim. Acta **282**: 340–356.

Hawco, N. J., and others. 2021*a*. Iron depletion in the deep chlorophyll maximum: Mesoscale eddies as natural iron fertilization experiments. Global Biogeochem. Cycl. **35**: e2021GB007112.

Hawco, N. J., F. Fu, N. Yang, D. A. Hutchins, and S. G. John. 2021*b*. Independent iron and light limitation in a low-light-adapted *Prochlorococcus* from the deep chlorophyll maximum. ISME J. **15**: 359–362.

Hayes, C. T., R. F. Anderson, M. Q. Fleisher, S. Serno, G. Winckler, and R. Gersonde. 2013. Quantifying lithogenic inputs to the North Pacific Ocean using the long-lived thorium isotopes. Earth Planet. Sci. Lett. **383**: 16–25.

Hayes, C. T., J. N. Fitzsimmons, E. A. Boyle, D. McGee, R. F. Anderson, R. Weisend, and P. L. Morton. 2015. Thorium isotopes tracing the iron cycle at the Hawaii Ocean Time-Series Station ALOHA. Geochim. Cosmochim. Acta **169**: 1–16.

Henderikx-Freitas, F., D. M. Karl, K. M. Björkman, and A. E. White. 2021. Constraining growth rates and the ratio of living to nonliving particulate carbon using beam attenuation and adenosine-5′-triphosphate at StationALOHA. Limnol. Oceanogr. Lett **6**: 243–252.

Hering, J. G., and F. M. M. Morel. 1989. Slow coordination reactions in seawater. Geochim. Cosmochim. Acta **53**: 611–618.

Hogle, S. L., and others. 2022. Siderophores as an iron source for *Prochlorococcus* in deep chlorophyll maximum layers of the oligotrophic ocean. ISME J **16**: 1636–1646. doi:10.1038/s41396-022-01215-w

Hudson, R. J. M., and F. M. M. Morel. 1990. Iron transport in marine phytoplankton: Kinetics of cellular and medium coordination reactions. Limnol. Oceanogr. **35**: 1002–1020.

Hutchins, D. A., A. E. Witter, A. Butler, and G. W. Luther. 1999. Competition among marine phytoplankton for different chelated iron species. Nature **400**: 858–861.

Hyslop, N. P., K. Trzepla, C. D. Wallis, A. K. Matzoll, and W. H. White. 2013. A 23-year record of twice-weekly aerosol composition measurements at Mauna Loa Observatory. Atmos. Environ. **80**: 259–263.

Ito, A., and others. 2019. Pyrogenic iron: The missing link to high iron solubility in aerosols. Sci. Adv. **5**: eaau7671.

Johnson, K. S., Riser, S. C., and Karl, D. M. 2010. Nitrate supply from deep to near-surface waters of the North Pacific subtropical gyre. Nature. **465**: 1062–1065. doi:10.1038/nature09170

Karl, D. M., J. R. Christian, J. E. Dore, D. V. Hebel, R. M. Letelier, L. M. Tupas, and C. D. Winn. 1996. Seasonal and interannual variability in primary production and particle flux at Station ALOHA. Deep Sea Res. Part II Top. Stud. Oceanogr. **43**: 539–568.

Karl, D. M., R. M. Letelier, R. R. Bidigare, K. M. Björkman, M. J. Church, J. E. Dore, and A. E. White. 2021. Seasonal-to-decadal scale variability in primary production and particulate matter export at Station ALOHA. Prog. Oceanogr. **195**: 102563. doi:10.1016/j.pocean.2021.102563

Keeling, C. D., Brix, H., and Gruber, N. 2004. Seasonal and long-term dynamics of the upper ocean carbon cycle at Station ALOHA near Hawaii. Global Biogeochem Cycles. **18**. doi:10.1029/2004GB002227

Kok, J. F., and others. 2021. Improved representation of the global dust cycle using observational constraints on dust properties and abundance. Atmos. Chem. Phys. **21**: 8127–8167. doi:10.5194/acp-21-8127-2021

Laglera, L. M., and M. Filella. 2015. The relevance of ligand exchange kinetics in the measurement of iron speciation by CLE–AdCSV in seawater. Mar. Chem. **173**: 100–113.

Lamborg, C. H., K. O. Buesseler, and P. J. Lam. 2008. Sinking fluxes of minor and trace elements in the North Pacific Ocean measured during the VERTIGO program. Deep Sea Res. Part II Top. Stud. Oceanogr. **55**: 1564–1577.

Letelier, R. M., R. R. Bidigare, D. V. Hebel, M. Ondrusek, C. D. Winn, and D. M. Karl. 1993. Temporal variability of phytoplankton community structure based on pigment analysis. Limnol. Oceanogr. **38**: 1420–1437.

Lis, H., Y. Shaked, C. Kranzler, N. Keren, and F. M. M. Morel. 2015. Iron bioavailability to phytoplankton: An empirical approach. ISME J. **9**: 1003–1013.

Liu, X., and F. J. Millero. 2002. The solubility of iron in seawater. Mar. Chem. **77**: 43–54.

Maldonado, M. T., and N. M. Price. 1999. Utilization of iron bound to strong organic ligands by plankton communities in the subarctic Pacific Ocean. Deep Sea Res. Part II Top. Stud. Oceanogr. **46**: 2447–2473.

Menden-Deuer S., and Lessard, E. J. 2000. Carbon to volume relationships for dinoflagellates, diatoms, and other protist plankton. Limnol Oceanogr. **45**: 569–579. doi:10.4319/lo.2000.45.3.0569

Mruwat, N., and others. 2021. A single-cell polony method reveals low levels of infected *Prochlorococcus* in oligotrophic waters despite high cyanophage abundances. ISME J. **15**: 41–54.

Murray, J. W., J. N. Downs, S. Strom, C.-L. Wei, and H. W. Jannasch. 1989. Nutrient assimilation, export production and ^{234}Th scavenging in the eastern equatorial Pacific. Deep Sea Res. Part A. Oceanogr. Res. Pap. **36**: 1471–1489.

Nishioka, J., H. Obata, H. Ogawa, K. Ono, Y. Yamashita, K. Lee, S. Takeda, and I. Yasuda. 2020. Subpolar marginal seas fuel the North Pacific through the intermediate water at the termination of the global ocean circulation. Proc. Natl. Acad. Sci. **117**: 12665–12673.

Pham, A. N., A. L. Rose, A. J. Feitz, and T. D. Waite. 2006. Kinetics of Fe (III) precipitation in aqueous solutions at pH 6.0–9.5 and 25°C. Geochim. Cosmochim. Acta **70**: 640–650.

Pinedo-González, P., and others. 2020. Anthropogenic Asian aerosols provide Fe to the North Pacific Ocean. Proc. Natl. Acad. Sci. **117**: 27862–27868.

Pinedo-González, P., R. F. Anderson, S. M. Vivancos, F. J. Pavia, and M. Q. Fleisher. 2021. A new method to extract ^{232}Th, ^{230}Th and ^{231}Pa from seawater using a bulk-extraction technique with Nobias PA-1 chelating resin. Talanta **223**: 121734.

Planquette, H., and R. M. Sherrell. 2012. Sampling for particulate trace element determination using water sampling bottles: Methodology and comparison to in situ pumps. Limnol. Oceanogr. Methods **10**: 367–388.

Price, N. M., B. A. Ahner, and F. M. M. Morel. 1994. The equatorial Pacific Ocean: Grazer-controlled phytoplankton populations in an iron-limited ecosystem 1. Limnol. Oceanogr. **39**: 520–534.

Prospero, J. M., D. L. Savoie, and R. Arimoto. 2003. Long-term record of nss-sulfate and nitrate in aerosols on Midway Island, 1981–2000: Evidence of increased (now decreasing?) anthropogenic emissions from Asia. J. Geophys. Res. Atmos. **108**: AAC-10.

Rafter, P. A., D. M. Sigman, and K. R. M. Mackey. 2017. Recycled iron fuels new production in the eastern equatorial Pacific Ocean. Nat. Commun. **8**: 1–10.

Raven, J. A. 1990. Predictions of Mn and Fe use efficiencies of phototrophic growth as a function of light availability for growth and of C assimilation pathway. New Phytol. **116**: 1–18. doi:10.1111/j.1469-8137.1990.tb00505.x

Resing, J. A., P. N. Sedwick, C. R. German, W. J. Jenkins, J. W. Moffett, B. M. Sohst, and A. Tagliabue. 2015. Basin-scale transport of hydrothermal dissolved metals across the South Pacific Ocean. Nature **523**: 200–203.

Rii, Y. M., D. M. Karl, and M. J. Church. 2016. Temporal and vertical variability in picophytoplankton primary productivity in the North Pacific Subtropical Gyre. Mar. Ecol. Prog. Ser. **562**: 1–18. doi:10.3354/meps11954

Rose, A. L., and T. D. Waite. 2003. Kinetics of hydrolysis and precipitation of ferric iron in seawater. Environ. Sci. Technol. **37**: 3897–3903.

Schmidt, M. A., and D. A. Hutchins. 1999. Size-fractionated biological iron and carbon uptake along a coastal to offshore transect in the NE Pacific. Deep Sea Res. Part II Top. Stud. Oceanogr. **46**: 2487–2503.

Shaked, Y., K. N. Buck, T. Mellett, and M. T. Maldonado. 2020. Insights into the bioavailability of oceanic dissolved Fe from phytoplankton uptake kinetics. ISME J. **14**: 1182–1193.

Shaked, Y., B. S. Twining, A. Tagliabue, and M. T. Maldonado. 2021. Probing the bioavailability of dissolved iron to marine eukaryotic phytoplankton using in situ single cell iron quotas. Global Biogeochem. Cycl. **35**: e2021GB006979.

Shelley, R. U., W. M. Landing, S. J. Ussher, H. Planquette, and G. Sarthou. 2018. Regional trends in the fractional solubility of Fe and other metals from North Atlantic aerosols (GEOTRACES cruises GA01 and GA03) following a two-stage leach. Biogeosciences **15**: 2271–2288.

Shire, D. M., and A. B. Kustka. 2015. Luxury uptake, iron storage and ferritin abundance in *Prochlorococcus marinus* (Synechococcales) strain MED4. Phycologia **54**: 398–406.

Tagliabue, A., and others. 2016. How well do global ocean biogeochemistry models simulate dissolved iron distributions? Global Biogeochem. Cycl. **30**: 149–174.

Tagliabue, A., A. R. Bowie, P. W. Boyd, K. N. Buck, K. S. Johnson, and M. A. Saito. 2017. The integral role of iron in ocean biogeochemistry. Nature **543**: 51–59.

Tortell, P. D., M. T. Maldonado, and N. M. Price. 1996. The role of heterotrophic bacteria in iron-limited ocean ecosystems. Nature **383**: 330–332.

White, A. E., R. M. Letelier, A. L. Whitmire, B. Barone, R. R. Bidigare, M. J. Church, and D. M. Karl. 2015. Phenology of particle size distributions and primary productivity in the N orth P acific subtropical gyre (S tation ALOHA). J. Geophys. Res. Ocean. **120**: 7381–7399.

White, A. E., K. S. Watkins-Brandt, and M. J. Church. 2018. Temporal variability of *Trichodesmium* spp. and diatom-diazotroph assemblages in the North Pacific subtropical gyre. Front. Mar. Sci. **5**: 27.

Wilson, S. T., and others. 2017. Coordinated regulation of growth, activity and transcription in natural populations of the unicellular nitrogen-fixing cyanobacterium Crocosphaera. Nat. Microbiol. **2**: 1–9.

Witter, A. E., and G. W. Luther III. 1998. Variation in Fe-organic complexation with depth in the Northwestern Atlantic Ocean as determined using a kinetic approach. Mar. Chem. **62**: 241–258.

Witter, A. E., B. L. Lewis, and G. W. Luther III. 2000. Iron speciation in the Arabian Sea. Deep Sea Res. Part II Top. Stud. Oceanogr. **47**: 1517–1539.

Ye, Y., and C. Völker. 2017. On the role of dust-deposited Lithogenic particles for iron cycling in the tropical and subtropical Atlantic. Global Biogeochem. Cycl. **31**: 1543–1558.

Acknowledgments

The authors thank Angelicque White, Matthew Church and Erica Goetze for organizing and leading the EAGER Chief Scientist training cruise, which was funded by the National Science Foundation (1911990), as well as the Captain and crew of the R/V *Kilo Moana*. The authors also thank Tara Clemente, Adam Subhas, and Ashely Maloney for assistance with deployments at sea, Macarena Burgos for help with GOP measurements, and Tim Conway for assistance with MC-ICPMS analysis. This work was also supported by the Simons Foundation (602538 and 823167 to N.J.H., 329108 to S.G.J) and National Science Foundation grants 2022969 to N.J.H. and 1911990 to S.F.

Conflict of interest

None declared.

Submitted 16 March 2022
Revised 09 July 2022
Accepted 06 August 2022

Associate editor: Vanessa Hatje